

# Technical note: Determining Arctic Ocean halocline and cold halostad depths based on vertical stability

Enrico P. Metzner<sup>1</sup> and Marc Salzmann<sup>1</sup>

<sup>1</sup>Institute for Meteorology, Universität Leipzig, Leipzig, Germany,

**Correspondence:** Enrico P. Metzner (enrico.metzner@uni-leipzig.de)

**Abstract.** The Arctic Ocean halocline separates the cold surface mixed layer (SML) from the underlying warm Atlantic Water (AW), and thus provides a precondition for sea ice formation. Here, we introduce a new method in which the halocline base depth is diagnosed from vertical stability and compare it to two existing methods. Our main motivation for diagnosing the halocline base depth based on vertical stability was that vertical stability is closely related to vertical mixing and heat exchange, and thus also to the role of the halocline in preventing vertical heat exchange and thereby protecting sea ice from warm AW. The second goal was to provide a particularly robust method. When applied to measurements from ice-tethered profilers, ships, and moorings, the new method for estimating the halocline base depth provides robust results with few artifacts. Comparatively large differences between the methods for detecting the halocline base depth were found in warm AW inflow regions for which climate models predict increased net surface energy fluxes from the ocean to the atmosphere, suggesting that these regions may be particularly sensitive to a halocline retreat. Analyzing a case in which water previously homogenized by winter convection was capped by fresh water at the surface suggests that the new method captured the beginning of new halocline formation in the Eurasian Basin. We also propose a novel method for detecting the cold halostad (CHS), which is formed by Pacific Winter Water (PWW) in the Canada Basin or by melt water off the eastern coast of Greenland and also Svalbard.

## 1 Introduction

The Arctic Ocean outside the main Atlantic warm water inflow and the shallow marginal shelf seas is usually stratified into a cold and fresh surface mixed layer (SML), which is from  $\sim 5$  to  $>100$  m thick, depending on region and season (Peralta-Ferriz and Woodgate, 2015), a halocline below the SML with a base depth  $\sim 40$  to  $>200$  m (Fig. 4 of Polyakov et al., 2018), a layer of warm and saline Atlantic Water (AW) below the halocline centered near 300 to 500 m in the Eurasian Basin and somewhat deeper in the Canada Basin (Aagaard et al., 1981; Macdonald et al., 2015), and deep water below. Convection in the SML is driven by surface cooling and brine release during sea ice formation, with maximum SML depth in winter. River inflow and precipitation act as sources of fresh water. Below the SML, salinity increases in the halocline. Within the halocline, one can distinguish between the cold halocline layer (CHL) in the Eurasian Basin, the Pacific Halocline Waters (PHW, modified Pacific Water which originally entered the western Arctic via the Bering Strait) in the Amerasian Basin, and the lower halocline waters (LHW, water of Atlantic origin which is less modified compared to CHL water) (e.g. Alkire et al., 2017; Polyakov et al., 2018; Anderson et al., 2013). In the CHL, the temperature remains close to the freezing point. Several processes have been suggested

as contributors to LHW and CHL formation. Based on data from the *Oden* 1991 cruise, Rudels et al. (1996) found that new halocline formation was initiated by the advection of relatively fresh shelf waters near the surface above denser and more saline water below, when the advection of the fresh water limited winter convection. Support for the importance of such a capping process was provided by Alkire et al. (2017) and Rudels et al. (2004). They argued that capping by fresh water due to sea ice melting in the inflow from the Fram Strait and the Barents Sea can transform AW into halocline water. Another process which has been widely discussed, and which is thought to be especially important for the PHW is the advection of dense and saline shelf waters (where salinity increases due to brine release during sea ice formation especially in winter) below the SML (Aagaard et al., 1981; Jones and Anderson, 1986; Rudels et al., 2004). While halocline formation via capping does not require dense shelf waters, capping can also occur after (i.e. in addition to) the advection of dense shelf water (Steele and Boyd, 1998; Rudels et al., 2004). Steele and Boyd (1998) argued that seasonal capping by melt water in summer may not be overly important for insulating the SML from relatively warm AW. The PHW in the Canada Basin originates from Pacific Water inflow, which is modified on the Chukchi Sea Shelf, but the LHW is of Atlantic origin also in the Canada Basin (e.g. Anderson et al., 2013). Because of seasonal modifications on the Chukchi Sea Shelf, the PHW in the Canada Basin can be further subdivided into Pacific Winter Water (PWW) and less saline and warmer Pacific Summer Water (PSW) (e.g. Timmermans et al., 2014). The PWW could be referred to as a type of cold halocline water (Zhong et al., 2019), although compared to the CHL in the Eurasian Basin, in the PWW, the salinity is lower and the salinity gradient is smaller. This is why Shimada et al. (2005) called the layer which is formed by PWW a cold halostad (CHS). Similarly, interaction between glacial melt water and Arctic water north east of Greenland forms an intermediate low salinity layer with small salinity gradient which is also called a cold halostad (Dmitrenko et al., 2017). Below, we argue that a lower salinity and a smaller salinity gradient in the CHS compared to the LHW below results in two distinct local stability maxima between the base of the LHW and the SML base: The upper stability maximum is associated with an increase of salinity in the upper PWW. The lower stability maximum is associated with another increase of salinity in the LHW. The lower one of these two stability maxima is absent in the presence of a CHL in the Eurasian Basin (except in regions off the eastern coast of Greenland and also Svalbard where melt water also forms a CHS).

Because density is more influenced by salinity than temperature if the temperature is low (Aagaard et al., 1981; Roquet et al., 2022) a configuration with warm AW underlying colder halocline water is stable. The presence of a (cold) halocline thus insulates the SML from direct contact with the warm AW and protects sea ice from the warm AW (Aagaard et al., 1981; Lind et al., 2016; Polyakov et al., 2017, 2020). Conversely, a retreat of the CHL in the Eurasian Basin leads to increased vertical mixing as observed and described by Steele and Boyd (1998); Björk et al. (2002); Polyakov et al. (2017). Retreating sea ice, increased surface heat flux and the retreat of the halocline have been called atlantification of the Eurasian Basin (Polyakov et al., 2017). Future climate model projections for a high emission scenario also showed very large temperature gradients directly below the surface mixed layer more frequently, especially during the cold season. The associated heating of the SML in combination with sea ice loss resulted in further increased annual mean upward net surface energy fluxes outside the Central Arctic along the main warm water inflow pathways (Metzner et al., 2020). While the halocline generally protects sea ice, PSW can be warm enough to participate in sea ice melting (e.g. Timmermans et al., 2014).

60 Several methods have been proposed for identifying the halocline based on observations. Steele et al. (1995) identified cold halocline water based on conditions for salinity ( $34 < S < 34.5$  in the practical salinity scale) and temperature ( $T < -0.5^{\circ}\text{C}$ ). Rudels et al. (1996) defined the boundaries of the CHL by using the 34.3 isohaline. Bourgain and Gascard (2011) used a density ratio threshold to define the base of the halocline. The density ratio is the ratio of temperature and salinity contributions to the vertical stability. A large density ratio implies that the vertical stratification is dominated by temperature and a small density ratio implies that stratification is dominated by salinity. The density ratio threshold suggested by Bourgain and Gascard (2011) assumes that oceanic layers above the halocline base are almost entirely salt-stratified with temperature contributing less than 5% to the total stratification (Polyakov et al., 2018). This density ratio method was adopted among others by others by Polyakov et al. (2017, 2018) and Metzner et al. (2020). Using tracer observations in the western Eurasian Basin, Bertosio et al. (2020) found the base of the LHW to be located at a density of  $1027.85 \text{ kg m}^{-3}$ . Analyzing salinity and temperature observations from 70 the Makarov Basin and along the East Siberian continental slope, Bertosio et al. (2022) again defined the base of the halocline using a density threshold and compared the results obtained with this definition to those obtained with other definitions from the literature. A fairly simple and robust method for computing the CHL base depth was proposed by Metzner et al. (2020). In this method, the base of the CHL is determined by a temperature difference of  $1^{\circ}\text{C}$  between water potential temperature and its freezing temperature. This temperature difference method is very sensitive to warming from below, while the density-ratio method of Bourgain and Gascard (2011) is very sensitive to the salinity profile. One drawback of the temperature difference method is a potential dependence of the optimal threshold value on region (Metzner et al., 2020). Polyakov et al. (2018) proposed an indicator of the potential of the Arctic halocline to prevent vertical mixing based on available potential energy, adapting the density ratio threshold of Bourgain and Gascard (2011) to identify the halocline base.

Here, we propose a new method to identify the halocline base using a vertical stability threshold and compare it to two 80 existing methods using measurements from ice-tethered profilers, ships, and moorings. Our main objective was to devise a method that uses a threshold value of a variable which is closely related to the role the halocline plays for insulating the SML from the warm AW. The choice of a vertical stability threshold was motivated by the argument that vertical stability is more directly related to vertical mixing than either density, temperature, or the density ratio. Our second goal was to devise a particularly robust method to detect the halocline base. Based on the argument that the presence of PWW forming a CHS on top of LHW creates a stability profile with two distinct local stability maxima, we also propose a method for estimating the 85 boundaries and the center of the CHS. Consistent and robust descriptions of the halocline and cold halostad layer boundaries are important to understand the evolution of the structure of the upper Arctic Ocean in the past and the future.

In the next section, we first describe methods to determine the halocline base depth, starting with two existing methods which are used for comparison, i.e. the density ratio (DR) method by Bourgain and Gascard (2011), and the temperature difference 90 (TD) method by Metzner et al. (2020). We then introduce our new stability (ST) method for determining the halocline base depth. In Section 2.2, we propose a new method for estimating the CHS upper and lower boundaries and the CHS center, which is based on vertical stability as well. In Section 2.3, we describe a method for estimating the SML base depth because the downward search for the DR and the TD threshold starts at the SML base and because the top of the halocline is assumed to coincide with the SML base. In Sect. 2.4, we introduce observational datasets used for comparison and testing. In Sect. 3,

95 we compare the new ST method for determining the halocline base depth to the existing methods and test the new method for  
determining the CHS depth and extent. We first compare the methods to determine the halocline base using case studies and  
investigate whether the ST method captures the beginning of new halocline formation based on a suggestion in a reviewer  
comment on the original submission by Polyakov (2023) in Sect. 3.1. We then use maps and basin-wise statistics (based on a  
suggestion in a reviewer comment by Athanase, 2023) in Sect. 3.2. The performance of the CHS algorithm is discussed in  
100 Sect. 3.3. The results are summarized and discussed Sect. 4.

## 2 Methods and Data

### 2.1 Methods for estimating the halocline base depth

#### 2.1.1 Density ratio (DR) method

In a halocline, the density gradient due to temperature must be small compared to the density gradient due to salinity by  
105 definition (Bourgain and Gascard, 2011). The density ratio (DR) method by Bourgain and Gascard (2011) therefore identifies  
the halocline base by the requirement that the ratio  $R_\rho$  between the density gradient due to temperature and the density gradient  
due to salinity must remain below a certain threshold. The density ratio is defined as  $R_\rho = (\alpha \nabla_z \theta) / (\beta \nabla_z S)$  with potential  
temperature  $\theta$  in °C, salinity  $S$  in the practical salinity scale and depth  $z$  in m.  $\alpha = -\rho^{-1}(\partial\rho/\partial\theta)$  and  $\beta = \rho^{-1}(\partial\rho/\partial S)$  are  
the thermal expansion coefficient and the haline contraction coefficient, respectively. Bourgain and Gascard (2011) empirically  
110 estimated that searching downward for the depth, in which  $R_\rho$  exceeds 0.05, provides a reasonable estimate for the base of  
the halocline. The search starts at the base of the SML (here determined as described in Sect. 2.3 below), which is defined to  
be the top of the halocline layer. If the density ratio threshold is exceeded already directly at the base of the SML, then no  
halocline was detected for the corresponding profile. Such profiles are excluded when computing statistics of halocline base  
depths. Similarly to Bourgain and Gascard (2011), we smoothed the  $S$  and  $\theta$  prior to computing the density ratio as explained  
115 in Sect. 2.4.

#### 2.1.2 Temperature difference (TD) method

The temperature difference (TD) method (Metzner et al., 2020) uses the difference  $\Delta T$  between the ocean temperature  $T$  and  
the sea water freezing temperature  $T_{\text{freeze}}$  to estimate the cold halocline base depth. The freezing temperature was calculated  
from Gill (1982). Searching downward, starting at the SML base, the base of the halocline was calculated as the depth, in  
120 which  $\Delta T$  first exceeds 1 K. This threshold was estimated to be high enough, that the "cold" core of the cold halocline layer is  
detectable, and low enough to separate the CHL from the AW with core temperature approximately 1.5°C to 3°C ( $T_{\text{freeze}} \approx$   
 $-2^\circ\text{C}$  leads to  $\Delta T \approx 3.5^\circ\text{C}$  to  $5^\circ\text{C}$  at the core). In cases in which the temperature threshold was first exceeded in a depth  
shallower than 80 m, the search was continued 0.5 m below this depth. If the temperature threshold was exceeded already at  
the SML base, no halocline was detected. The algorithm was applied to smoothed temperature data (see Sect. 2.4).

### 125 2.1.3 Stability (ST) method

The new stability (ST) method prescribes a threshold for the local vertical stability in order to estimate the halocline base depth. Vertical stability is more closely related to vertical mixing than either the density ratio or the temperature difference. Because the search direction was found to affect the robustness of the method, and because stability is decreasing with depth between the AW and the core of the halocline, we search upward instead of downward for the stability threshold. The stability  
 130 was computed from  $L = \log_{10}(N^2)$ , where  $N = \sqrt{-(g/\rho)(\partial\rho/\partial z)}$  is the Brunt-Väisälä-frequency (with density computed from pressure, smoothed  $S$ , and  $\theta$  as described below). The stability threshold was approximated based on the density ratio threshold  $R_\rho = 0.05$  assuming an approximately constant salinity gradient near the halocline base in the LHW. It was derived starting from the following relationship:

$$\rho^{-1}\nabla_z\rho = \beta\nabla_zS - \alpha\nabla_z\theta = \beta\nabla_zS(1 - R_\rho) \quad (1)$$

135 With stable  $\beta = (7.82 \pm 0.03) \cdot 10^{-4}$  over a wide range of temperature, salinity and pressure values ( $-1.2 \dots 2.0^\circ\text{C}$ ,  $32 \dots 37$ ,  $50 \dots 350$  dbar) and the salinity gradient in  $\text{m}^{-1}$ :

$$L = \log_{10}(-\nabla_zS) - 2.137 \pm 0.002 \quad (2)$$

Expecting the salinity gradient to be around  $0.01 \text{ m}^{-1}$  near the base of the halocline, the resulting stability threshold should be  $L \approx -4.14$ .

140 This threshold is searched from 600 m or at the lowest point (at least 500 m deep outside the shallower regions according to the conditions for including profiles in the analyses described below in Sect. 2.4) to the surface, as no CHL base was observed deeper than that. Seldom, the first estimate is in warm AW at  $T > 0^\circ\text{C}$ . In such cases, a second search for the stability threshold is started slightly above. If the stability threshold is never exceeded or only exceeded where  $T > 0^\circ\text{C}$  in a given profile, then no halocline base was detected for this profile.

### 145 2.2 Cold halostad (CHS) boundary and center estimates

A CHS is formed by PWW in the Canada Basin and also by melt water off the eastern coast of Greenland and Svalbard. Compared to the CHL in the Eurasian Basin, a CHS is characterized by a smaller salinity gradient because of the different water origins. As demonstrated below, this leads to one local stability maximum at the top of the CHS (at the transition between SML or PSW and PWW) and a second stability maximum associated with the transition between CHS and the LHW. The stability  
 150 minimum between these two local stability maxima is associated to the CHS. Therefore, as a first condition for identifying a CHS, we require that more than one local stability maximum must be present between the base of the SML and the base of the halocline as identified by the ST algorithm described above. Because the stability profiles computed from temperature and salinity observations contain small scale fluctuations even after smoothing the  $S$  and  $\theta$  data that is used for computing density as described below, we identify local maxima by first computing a “moving” stability maximum for a 50 m vertical box  
 155 surrounding each observation. This moving stability maximum is computed from  $L_m(z) = \max(L(z'))$  for  $|z' - z| < 25$  m),

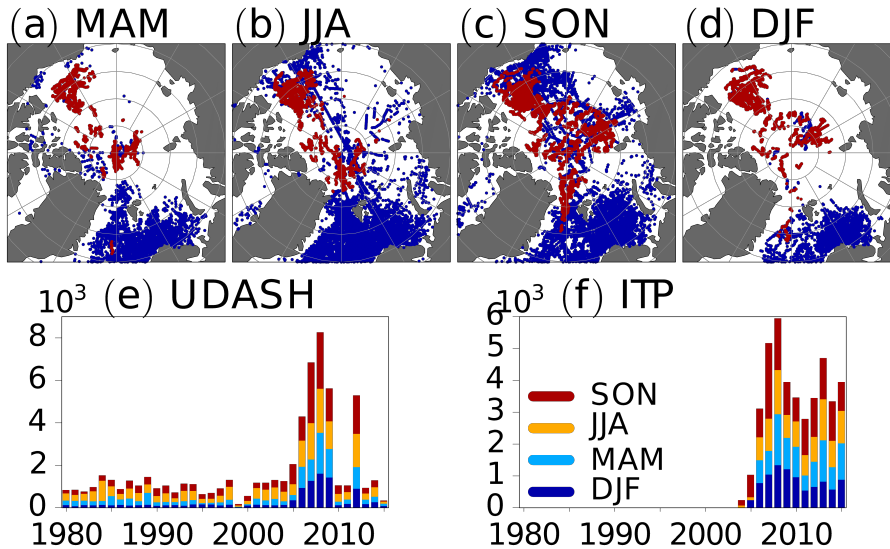


**Figure 1.** Locations of observations for each season (starting with MAM for March, April, and May) with blue dots for UDASH profiles and red dots for ITP profiles (a–d). Temporal coverage for UDASH (e) and ITP (f) observations.

where  $z$  is depth. This moving maximum operation was defined in analogy to a moving average. The result is a profile of stability maxima  $L_m(z)$  with few local maxima. We then compute the mean of the lower stability maximum, which is associated with the transition between CHS and LHW, and the stability minimum between the upper and the lower stability maximum, which is associated with the CHS. This value is used as a threshold to define the upper and the lower boundary of the CHS.

160 The depth of the center of the CHS is defined as the mean of the upper and lower boundary of the CHS. A CHS will only be recognized by the algorithm if the vertical distance between the deeper stability maximum the first upper occurrence of that same stability value is at least 50m, and the difference of  $L$  between the lower stability maximum and the local minimum in the CHS is at least 0.2. With this definition, we never identified more than a single CHS per profile.

### 2.3 SML depth estimate

165 The SML depth was estimated by a change in potential density of  $0.125 \text{ kg m}^{-3}$  at the surface as in Polyakov et al. (2017). In cases, in which a CHL is detected, the depth of the SML corresponds to the top of the CHL. Potential density was computed from smoothed  $S$  and  $\theta$ .

### 2.4 Data and preprocessing

Temperature and salinity observations were taken from the ice tethered profiler (ITP) project (Krishfield et al., 2008; Toole et al., 170 2011) and the Unified Database for Arctic and Subarctic Hydrography (UDASH, Behrendt et al., 2018). The ITPs measured temperature, salinity, and pressure twice a day while drifting with the ice floe they were tethered to. Data processing for the ITP

data is described by Krishfield et al. (<http://www.whoi.edu/filesserver.do?id=35803&pt=2&p=41486>). Here, we used processed ITP Level III data. Producing Level III data included removal of corrupted data, corrections for the sensor response behavior, calibrations, and final screening of spurious outliers. ITPs deployed in the Arctic Ocean before 2018 were included here. The vertical resolution for ITP level III data is  $1 \pm 0.1$  dbar. The accuracy of the sensors used for the ITP observations is  $0.002^\circ\text{C}$  for temperature and 0.002 for salinity (Polyakov et al., 2017). The UDASH data set contains data from ships, ice-tethered profilers, profiling floats and other platforms (Behrendt et al., 2018). Only profiles, for which both temperature and salinity were available, were analyzed here. Furthermore, only profiles with a vertical resolution finer than 2.5 dbar in the upper 300 m and a vertical resolution finer than 5 dbar elsewhere were used. We also required that the deepest point in a profile must reach at least 500 m or 90% of the basin depth. This choice addresses the issue of potential sampling biases due to limited vertical extent of the observed profiles. Regions shallower than 100 m were always excluded from the analysis. Bathymetry data was taken from the General Bathymetric Chart of the Oceans (GEBCO) dataset (GEBCO Bathymetric Compilation Group 2021, 2021). This filtering left a total of 43715 ITP and 62012 UDASH profiles. Fig. 1 provides an overview of the spatio-temporal coverage of the data. Most measurements are concentrated in the Barents Sea and only few were taken in the Central Arctic during winter. For the East Siberian Sea and the interior of the Laptev Sea, no data was available for winter and spring. Salinity was given in the practical salinity scale.

Depth was computed from pressure using the hydrostatic equation. Density was computed based on salinity, temperature, and pressure. In order to reduce noise,  $S$ ,  $T$ , and/or  $\theta$  were smoothed using a standard one-dimensional Gaussian filter (convolution with a Gaussian function, e.g. Deng and Cahill, 1993) with a standard deviation of 2 dbar and a truncation at  $\pm 10$  dbar. When using thresholds to estimate the SML or CHL base depth, variables were linearly interpolated between two adjacent depths. Consequently, the SML or CHL base can be located between two vertical observation points and the SML and CHL base depths do not necessarily have to coincide with the depths of the observations.

### 3 Results

#### 3.1 Comparison of methods for deriving halocline base depth using case studies

Figure 2 compares three different methods for determining the halocline base depth for ITP-74. Starting from the Laptev Sea in September 2013, ITP-74 drifted across the Central Arctic, almost reaching the East Greenland Sea (Fig. 2a). Until May 2014, Fig. 2b–d shows evidence of a well-defined and stably stratified CHL below the SML. The vertical stratification observed by ITP-74 prior to May 2014 and the performance of the three methods for determining the halocline base depth are further analyzed in an individual profile from this period in Fig. 3. Individual profiles of salinity and temperature for 13 January 2014 in Fig. 3a show the base of the SML at about  $\sim 30$  m. Between the SML base and  $\sim 80$  m a strong salinity gradient and temperatures close to the freezing point indicate a well defined CHL, which is  $\sim 60$  m thick. Between the CHL and the AW, temperature and salinity increase in the LHW. Below  $\sim 170$  m warm and saline AW is found (please note that at  $\sim 170$  m, the temperature and salinity slopes in Fig. 3a both change). Figs 3b–d show the density ratio, the temperature difference, and the stability for the observations on 13 January 2014 together with the threshold values used to identify the halocline base with the

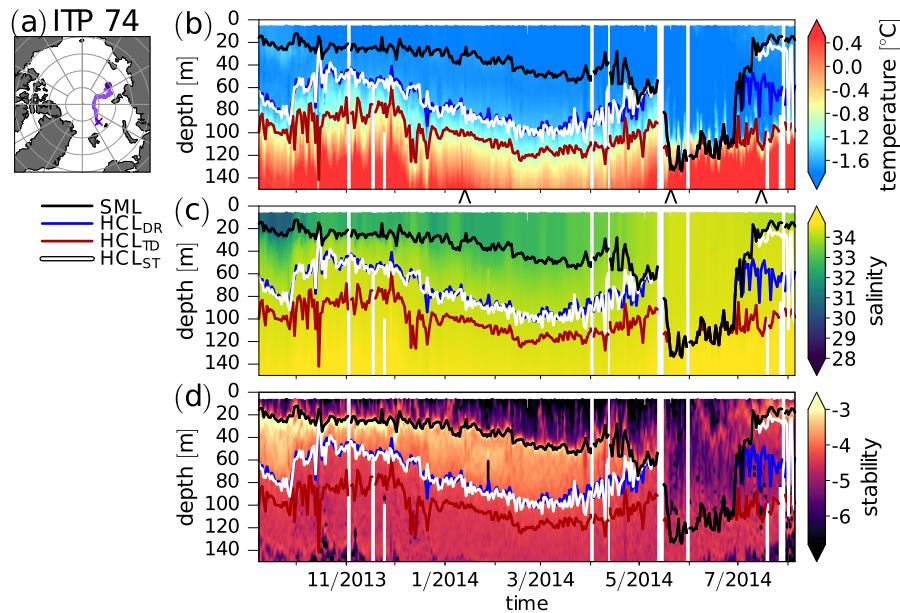


**Figure 2.** ITP-74 location of measurements (a) and time series of temperature (b), salinity (c), and vertical stability (d). The circle and the cross in (a) mark the beginning and the end of the ITP-74 track, respectively. The colored lines in (b–d) are the base of the SML (black) and the halocline (HCL) base depths derived by the DR method (blue), the TD method (red) and the ST method (white). Salinity is given in the practical salinity scale. Individual profiles at the location of the wedge symbols ( $\wedge$ ) below the x-axis in (b) are shown in Fig. 3. Profiles that started below 15 m were excluded (only) in this figure (but nowhere else), because this increased readability by reducing the effect of noise in determining the SML base without affecting the overall result.

205 DR, the TD, and the ST method. For the profile observed on 13 January 2014, the DR method (Fig. 3b) and the ST method (Fig. 3d) identify the CHL base, while the TD method (Fig. 3c) places the halocline base in the LHW, somewhere between CHL and AW. The stability profile in Fig. 3d yields distinctly different stabilities for the SML, the CHL, the LHW, and the AW.

In May 2014, the SML deepens and the CHL disappears (Figure 2), as previously noted by Polyakov et al. (2017). During this convection event, neither of the three methods identified a halocline. Figs 3e–h show profiles for 20 May 2014 after the onset of convection. On this date, the threshold for identifying the halocline base was already exceeded at the SML base for the DR and the TD method (Fig. 3f and g), while the threshold was not reached for the ST method (Fig. 3h). After July, the situation becomes particularly interesting. The stability at about 80 m depth remains low, pointing to the residual of a mixed layer well below the diagnosed SML base (Figure 2). Fig. 3i for 15 July 2014 (after convection) also shows freshening and warming near the surface. This indicates that relatively fresh melt or/and shelf water may have been advected above a colder and saline layer, which had previously been homogenized by winter convection. The freshening near the surface leads to a salinity gradient below, and also a stability maximum, which is captured by the ST method (Fig. 3h). This appears to be consistent with the mechanism for halocline formation described by Rudels et al. (1996). As stated above, Rudels et al. (1996) found new

215

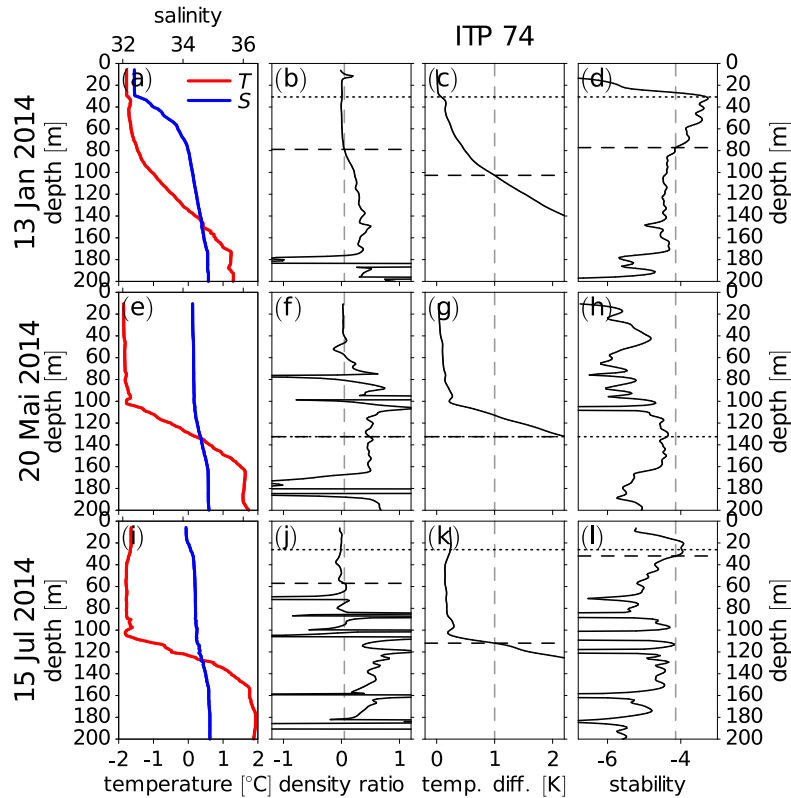


**Figure 3.** Temperature  $T$  and salinity  $S$ , density ratio, temperature difference, and stability from ITP-74 before winter convection on 13 January 2014 (a–d), during winter convection on 20 May 2014 (e–h) and after winter convection on 15 July 2014 (i–l). Vertical dashed lines indicated threshold values. Horizontal dashed lines indicate the halocline base determined by the three different methods. Dotted lines indicate the SML base. Dash-dotted lines in (f) and (g) indicate that a threshold for identifying the halocline base was exceeded at the SML base.

halocline formation taking place when relatively fresh shelf waters near the surface were advected above denser and saltier water below, limiting winter convection, while Rudels et al. (2004) and Alkire et al. (2017) stressed the role of melt water in general (including non-shelf water) in the warm Atlantic inflow through the Fram Strait and the Barents Sea for halocline formation via this type of capping mechanism. Fig. 2 suggests that in this particular case, the convection affected halocline water. This is also consistent with a study by Steele and Boyd (1998), who suggested that the capping mechanism can act in addition to the advection of dense and saline shelf waters. In the Steele and Boyd (1998) mechanism, which combines findings by Rudels et al. (1996) with earlier findings (e.g. Aagaard et al., 1981), high salinity in the capped water derives from advected cold and dense shelf water, which may previously have been affected by brine release in shelf seas, and not directly from AW. Here, the origin of the halocline water is unclear. However, Fig. 3h for 15 July 2014 (after winter convection) suggests that the ST method might indeed be useful for identifying the beginning of new halocline formation via the Rudels et al. (1996, 2004)

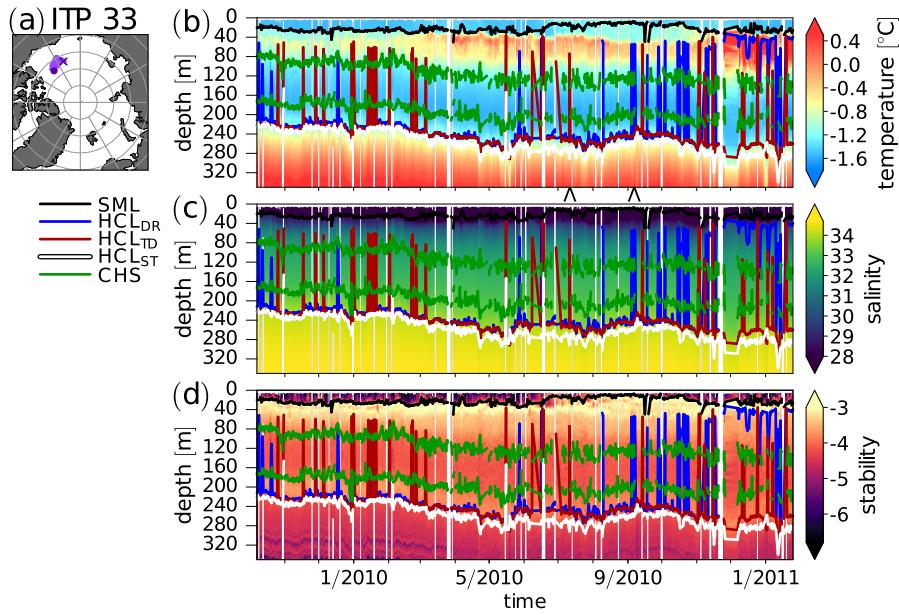


**Figure 4.** As Fig. 2 but for ITP-33. Additionally, the results of the cold halostad bound estimation are shown in dark green.

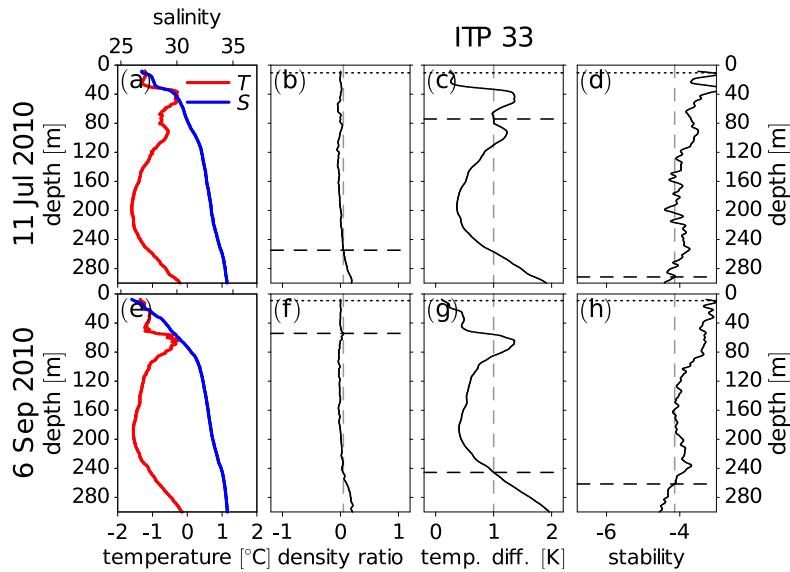


**Figure 5.** As Figure 3, but for two profiles from ITP-33. For 12 July 2010 (a–d) the TD method shows an isolated minimum of the halocline base depth, and for 6 September 2010 (e–f) the TD method shows an isolated minimum of the halocline base depth.

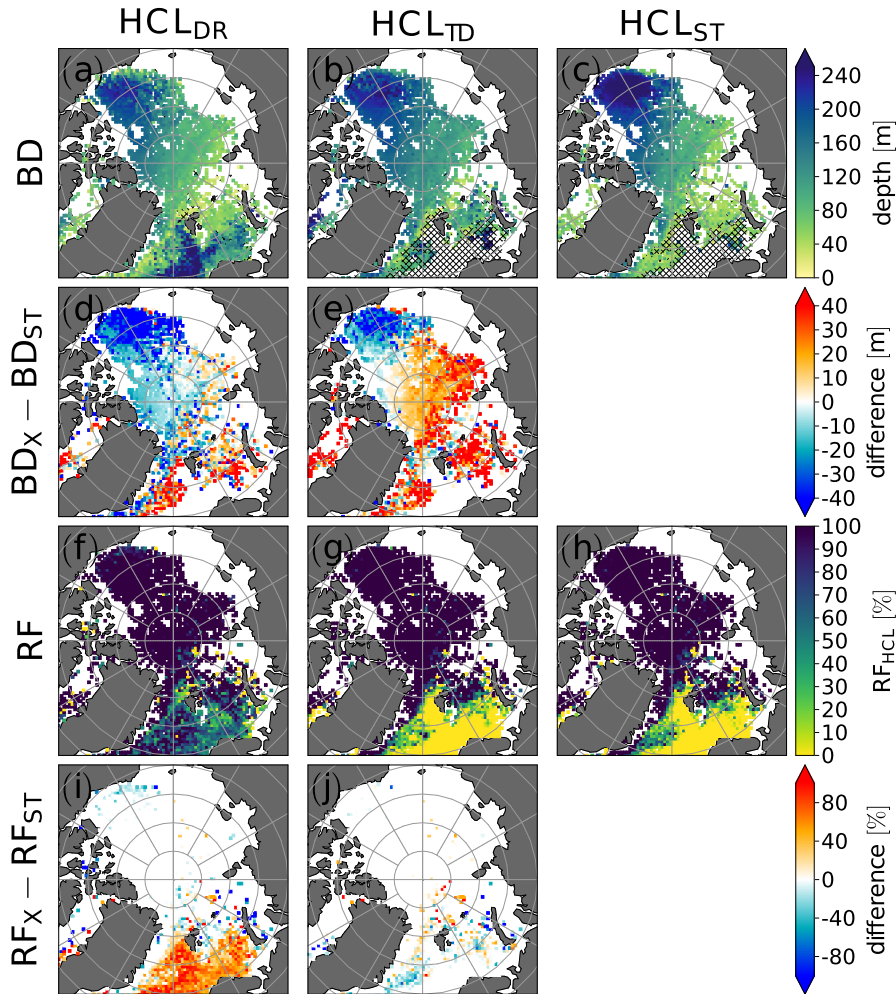
capping mechanism or the Steele and Boyd (1998) mechanism which essentially assumes that the Rudels et al. (1996) capping mechanism acts in addition to the advection of dense shelf water (e.g. Aagaard et al., 1981).

Figure 4 again compares the three different methods for determining the halocline base depth, but this time for ITP-33, which drifted in the Canada Basin between October 2009 and January 2011, where it encountered PSW on top of PWW. In addition to the halocline base depth, Fig. 4b–d shows the CHS boundaries which have been estimated based on stability as described above. The performance of the new algorithm for identifying the CHS will be discussed further below. For now, the main focus will be on isolated spurious minima of the halocline base depth. As evidenced by the spikes in Fig. 4b–d, such isolated spurious base depth minima occur for the DR and the TD algorithm, but not the ST algorithm. Reasons for the occurrence of these artifacts will be further analyzed based on Figure 5. Figure 5a–d shows a case from ITP-33 on 11 July 2010 in which the TD method produced an isolated halocline base depth minimum and Fig. 5e–f shows a case on 6 September 2010 in which the DR method produced an isolated halocline base depth minimum. In both cases, the isolated minima are related to a layer of warm PSW around  $\sim 80$  m (Figs. 5a and e, compare also Fig. 4b). For 11 July 2010, the best estimate of the halocline base depth is provided by the DR method (Fig. 5b). The DR method correctly places the base of the halocline water at a depth, where the salinity gradient (Fig. 5a) changes. Stability (Fig. 5d) also decreases markedly at this depth, although the ST method identifies the halocline base about 20 m below this location (Fig. 5d). The TD method (Fig. 5c) places the halocline base at about 80 m in the layer of warm PSW, although the salinity gradient below this layer still indicates the presence of a halocline and temperature decreases below this layer, indicating PWW. For 6 September 2010, the DR threshold is exceeded at a local density ratio maximum which is related to a very steep temperature gradient (Fig. 5f) at the base of the PSW. While all three methods rely on finding a threshold, the search direction differs. Because the ST method searches upward, the warm PSW layer does not result in isolated depth minima (Figs. 5d and h). Overall, this analysis suggests that the search direction matters. With the DR and the TD method, we search downward, while with the ST method we search upward. This helps to explain why the ST method yields more robust results with fewer unexpected depth minima appearing in the basin-wise statistics discussed below. For the DR method, on the other hand, Fig. 3a shows that the DR threshold is exceeded also far below the halocline base. Such local DR maxima below the halocline base were also found in the presence of thermohaline staircases (not shown here). Additional DR maxima below the halocline base, such as the one in Fig. 3, prevent us from simply reversing the search direction in the DR algorithm.

### 3.2 Statistical comparison of the halocline base depth and occurrence frequency from different methods

In order to identify differences between the methods used for halocline base detection regarding the geographical distribution of halocline base depth and halocline occurrence frequency (i.e. number of profiles for which a halocline base was detected divided by number of profiles analyzed) we used a simple nearest-neighbor (NN) averaging to produce maps (Fig. 6). The underlying grid uses an azimuthal-equidistant projection with  $\sim 0.47^\circ$  resolution at the North Pole. In addition to these maps (which in data-rich regions show a time mean halocline base depth), we computed basin-wise statistics of halocline base depths. Figure 7 shows relative frequencies of halocline base depth diagnosed with the three methods for the Eurasian Basin, the Makarov Basin, and the Canada Basin.

As expected, all three methods yield a similar overall spatial distribution of halocline base depth (Fig. 6a–c) with shallower halocline base in the Eurasian Basin and the Makarov Basin compared to the Canada Basin. This spatial pattern is consistent



**Figure 6.** Halocline base depth (BD) derived by the density-ratio (DR) algorithm (a), the temperature-difference (TD) algorithm (b), and the new stability (ST) algorithm (c). Difference of HCL BD between the DR and the ST algorithm (d) and between the TD and the ST algorithm (e). Relative frequency (RF) of HCL occurrence (i.e. number of profiles for which a halocline was detected divided by number of profiles analyzed) (f–h) and differences (i–j) as in (a–e). In (a–c), points where the relative occurrence frequency of the HCL was below 1% were masked out. Hatching indicates regions where the HCL occurrence frequency is below 25%. Points where the ocean floor depth is below 100 m were masked out.

265 with Polyakov et al. (2018). In the Eurasian Basin, the time averaged halocline base depth diagnosed with the DR method (Fig. 6a) and the ST method (Fig. 6c) agree relatively well, while the TD method overestimates halocline depth relative to both other methods (Fig. 6b). For the elliptical area covering the Eurasian Basin in Fig. 7a, the mean base depth was 85.9 m for the DR method and 92.3 m for the ST method vs. 116.1 m for the TD method. This overestimate of the halocline base depth

by the TD method compared to the other two methods is consistent with the previous result for ITP-74. Unlike the DR and the ST method, which both correctly identified the CHL base during the first months of ITP-74, the TD method placed the halocline base somewhere in the LHW. In addition to the moderate difference in the mean base depth between the DR and the ST method, the relative frequency of halocline base depth (Fig. 7b) in the Eurasian Basin reveals differences between the DR and the ST method, which are not reflected by the difference of the mean base depths. The ST method more often identifies a shallow halocline base ( $< 60$  m) in the Eurasian Basin compared to the DR method, which is consistent with the finding that the ST method apparently captures the start of new halocline formation from Sect. 3.1. More frequent detections of halocline bases not only above 60 m but also below 120 m with the ST method compared to the DR method account for a slightly wider halocline base depth distribution in the Eurasian Basin in the ST method compared to the DR method (Fig. 7b). The more frequent halocline base depths larger than 120 m in the ST method are likely related to an overestimate of halocline base depth similar to the one found for the ST method for ITP-33 above. Slightly increasing the stability threshold in the ST method may lead to a better match between the halocline base depth estimate from the ST and the TD method by moving the halocline base estimated by the ST method upward and by decreasing the sensitivity of the ST method to new halocline formation. For the elliptical area covering the Makarov Basin in Fig. 7b, the DR method yielded a mean halocline base depth of 112.3 m, the ST method of 118.1 m, and the TD method of 133.5 m. For the elliptical area covering the Canada Basin, on the other hand, the ST method yielded the largest mean halocline base depth. The mean halocline base depths for the Canada Basin corresponding to Fig. 7d are 191.4 m for the DR method, 206.6 m for the TD method, and 219.1 m for the ST method. In the Canada Basin (Fig. 7d), the ST method detected a halocline base shallower than 160 m for 0.05% of the profiles, while the DR method detected a halocline base shallower than 160 m for 10.2% of the profiles and the TD method for 3.5% of the profiles, indicative of isolated base depth minima due to the influence of warm PSW above PWW. Isolated minima very likely also contribute to a more variable (noisier) halocline base depth in the Canada Basin in the map for the DR method in Fig. 6a and to a lesser extent also in the map for the TD method in Fig. 6b compared to the ST method (Fig. 6c). The larger average base depth in the Canada Basin in the ST method compared to both other methods (see also Fig. 6d and e) is, however, not only explained by the isolated depth minima in the DR and the TD method in Fig. 7d. Instead, more frequent depths greater than 260 m in the ST method compared to the other two methods (Fig. 7d) contribute to the greater average halocline base depth diagnosed with the ST method, again indicating that a slight increase of the stability threshold in the ST method would lead to a better agreement between the halocline base depth from the ST and the DR method. While a halocline was almost always detected in the Canada Basin by all three methods, the relative occurrence frequency (defined as the number of profiles in which a halocline base was detected divided by the total number of profiles which were analyzed) varies strongly in the Norwegian Sea (Fig. 6f–h). While the ST method and also the TD method very rarely detected a halocline base in the Norwegian Sea, the DR method frequently detected a halocline base in the Norwegian Sea. Furthermore, the DR method suggests a transition from a deeper halocline in relatively warm water inflow to a shallower halocline further north, which is absent in the other two methods (Fig. 6a–c). When using the DR method for analyzing halocline retreat in these warm water inflow regions, this may lead to different results compared to the two other methods. One reason for the DR method detecting a halocline base at depth could be thermohaline staircases. Overall, the largest differences in halocline detection frequency between the methods (Fig. 6i and j) were found in

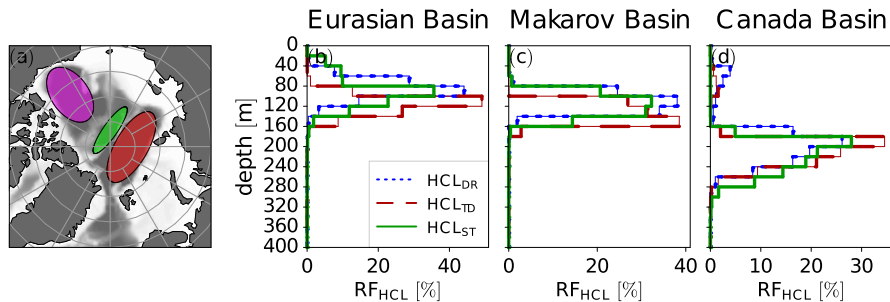


**Figure 7.** Map showing elliptical areas over the Canada Basin (purple), the Makarov Basin (green) and the Eurasian Basin (dark red) and ocean floor depth (grey shading) (a). Relative frequency of halocline (HCL) base depth determined with the density ratio (DR), temperature difference (DR) and the stability (ST) method for the elliptical areas over the Eurasian Basin (b), the Makarov Basin (c), and the Canada Basin (d).

regions which are prone to sea ice retreat and, according to global climate model results, may also be particularly prone to events, in which large temperature gradients are found directly underneath the SML, and which mainly occur during winter (Metzner et al., 2020). In order to prevent the DR method from identifying a halocline base in relatively warm water, one could either limit the region to which the method is applied (as Polyakov et al., 2018) or else introduce additional constraints on the water temperature. Limiting the region is clearly a sensible choice in a stable climate. However, limiting the region to a region in which a stable (cold) halocline is found at most times limits us in studying regional shifts. With regard to shifts due to climate change, one should be aware that methods differ regarding requirements for halocline base identification and results.

### 3.3 Estimation of cold halostad boundaries

In the Canada Basin, the PWW forms a so-called cold halostad, while the LHW is modified water of Atlantic origin. This leads to a local vertical stability minimum between two local vertical stability maxima (Fig. 5d and h). The upper vertical stability maximum is associated with an increase of salinity near the top of the PWW and the lower stability maximum is associated with an increase in salinity between PWW and LHW. The local minimum of vertical stability between these two local maxima is associated with a small salinity gradient around the core of the PWW (Fig. 5a and e). The new algorithm described in Sect. 2.2 was designed to provide estimates for the location of the cold halostad layer boundaries and the center, where the center is assumed to be the mean depth between the upper and the lower boundary. Top and base depth timeseries derived with the new algorithm are shown by dark green lines in Fig. 4. The algorithm was designed to avoid misclassifications of the cold halostad by requiring the difference between the lower stability maximum and the stability minimum (i.e. the depth of the 'stability valley') to be at least 0.2. Furthermore, the vertical extent of the 'stability valley' was required to be greater than 50m. This leads to occasional discontinuities in the cold halostad boundary. Fig. 4 shows such discontinuities as evidenced by the breaks in the dark green lines. Furthermore, the requirement of a minimum depth leads to shallow halostad layers not being detected.

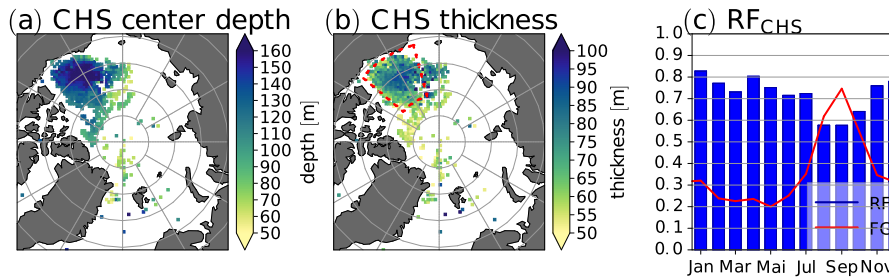


**Figure 8.** Map of mean (a) CHS center depth and (b) CHS thickness. (c) Monthly relative occurrence frequency ( $RF_{CHS}$ , blue bars) of the CHS in the Canada Basin region (area enclosed by red dashed lines in (b) and fraction of grid points (FG) for which at least one observation was available in the respective month (red line).

Collecting all available observations with detected cold halostad boundaries per grid cell leads to the maps of CHS center  
 325 depth and CHS thickness shown in Fig. 8a and b. The main occurrence region of the cold halostad is the Canada Basin,  
 where Pacific water circulates between the SML and water of Atlantic origin (Shimada et al., 2005). Employing conservative  
 assumptions to avoid a misclassification (including a lower bound of 50 m for the thickness), we detect a cold halostad layer  
 in the Canada Basin region in Fig. 8b  $\sim 70\text{--}90\%$  of the time, except in August, September, and October when the occurrence  
 frequency is slightly below 70% (Fig. 8c). In August, September, and October the fraction of grid points for which observations  
 330 were available within the Canada Basin region was also particularly high (red line in Fig. 8c). Based on Fig. 1, more points  
 at the edge of the Canada Basin region in Fig. 8b, where the occurrence frequencies decrease, may have been included in the  
 analysis during these month. Furthermore, a cold halostad was detected near the coasts of Greenland where glacial cold water  
 acts similar to the Pacific low salinity water (Dmitrenko et al., 2017).

#### 4 Summary and discussion

We introduced a new method for determining the halocline base depth based on vertical stability and compared it to the density  
 335 ratio and the temperature difference method. Our main motivation for using a vertical stability threshold instead of a DR or  
 TD threshold was that vertical stability is more closely related to the role of the halocline as a stable layer which separates the  
 SML from warmer AW below and thus acts to protect sea ice. Another objective was to design a particularly robust method.  
 We also devised a new stability-based method to identify the CHS, which is formed by PWW in the Canada Basin and also by  
 340 melt water off the eastern coast of Greenland and Svalbard. To our knowledge, this is the first time that a method for detecting  
 the CHS has been devised and tested.

We found that the DR and the new ST method both correctly identified the base of the CHL in the Eurasian Basin during  
 the first months of ITP-74, while the TD method placed the halocline base somewhere in the LHW. Furthermore, the analysis  
 of individual profiles after convection in ITP-74 indicated that the new ST method captured the beginning of new halocline  
 345 formation via the convective homogenization and subsequent fresh water capping mechanism proposed by Rudels et al. (1996).

In the Canada Basin, the new method overestimated the halocline base depth compared to the DR method, which correctly identified the halocline base for ITP-33. This disagreement between the DR and the ST method could be reduced by slightly increasing the stability threshold in the ST method. Slightly increasing the stability threshold (which is at present based on an approximate relationship between density ratio and stability) may lead to a better agreement of halocline base depth between the DR and the ST method not only by moving the halocline base from the ST method upward but also by decreasing the sensitivity of the ST method to new halocline formation.

Unlike the two existing methods, the new ST method to detect the halocline base yielded few artificial halocline base depth minima. In the two existing methods, such artifacts were found to be associated with warm PSW on top of cold PWW in the Canada Basin. Because the new method searches for the halocline base from below, such artifacts were avoided, leading to a more robust method, especially compared to the widely used DR method. Unfortunately, because of DR maxima below the cold halocline base (which are for example associated with thermohaline staircases), the search direction in the DR method cannot simply be reversed in order to increase the robustness also of the DR method.

A particularly striking difference between the DR method and the other two methods was found in the Norwegian Sea. While the ST and the TD method almost never detected a halocline in the Norwegian Sea, the DR method frequently detected a halocline base in the Norwegian Sea. Remarkably, the halocline in the DR method decreased north of the Norwegian Sea. This intriguing difference between the methods should be taken into account, for example when studying the effects of warm AW inflow on the cold halocline, especially because warm water inflow regions are particularly prone to react to anthropogenic warming (although the effects of warming on either accelerating or preventing new halocline formation are manifold and changing over time, and destabilization of an existing stable halocline by warming from below is only one potential contributor to increased annual mean net surface heat fluxes from the ocean to the atmosphere in warm water inflow regions found in climate models).

Regarding the new method for CHS detection, a case study and an application to a comprehensive dataset yielded encouraging results. The case study suggested that the method correctly identified a layer with a small vertical salinity gradient formed by PWW. This small salinity gradient led to a stability minimum between two local stability maxima which was captured by the new stability method for CHS detection. Because we found it necessary to introduce a constraint on the cold halostad thickness and to set a threshold requirement for the magnitude of the stability minimum, our method suffers from a low detection sensitivity and altogether misses cold halostad layers that are thinner than 50 m. Nevertheless, a cold halostad was frequently detected in the Canada Basin throughout the year and the number of missed detections tended to be small as for ITP-33, while some other ITPs yielded almost perfect results and some other ITPs slightly worse results (not shown). This suggests that a stability-based method for CHS detection could be useful for future studies exploring variability and changes of the CHS in the Canada Basin.

One method to advance cold halostad and halocline base detection in the future may lie in the application of artificial intelligence. This would require a-priori manual classification applied to a training and an evaluation dataset. In the absence of objective criteria that work under most circumstances, such manual classification would ultimately have to rely on expert

380 judgment, which may in turn introduce a different set of problems. Given the various shortcomings of traditional threshold  
methods, AI-based methods could nevertheless be useful.

*Code and data availability.* The Ice tethered profiler data (Krishfield et al., 2008; Toole et al., 2011) used in this paper are taken from  
the website of the Ice-Tethered Profiler program based on Woods Hole Oceanic institution via <https://www2.who.edu/site/itp/> (last access  
23 January 2022). The UDASH-dataset (Behrendt et al., 2018) is available from the PANGAEA data archive at [http://doi.org/10.1594/  
385 PANGAEA.872931](http://doi.org/10.1594/PANGAEA.872931).

*Author contributions.* E.P.M. devised the new method for determining the Arctic Ocean cold halocline and cold halostad layer depths and  
performed the data analysis. Both authors contributed equally to writing the manuscript.

*Competing interests.* The authors declare that they have no conflict of interest.

*Acknowledgements.* We thank the two reviewers, I. Polyakov and M. Athanase, for their very insightful and very constructive comments,  
390 especially for their suggestions regarding the analysis of individual profiles, new halocline formation, the structure of the introduction, and  
basin-wise statistics, which we consider a major contribution to our revised manuscript. The Ice-Tethered Profiler data were collected and  
made available by the Ice-Tethered Profiler Program based at the Woods Hole Oceanographic Institution (<http://www2.who.edu/site/itp/>).  
We gratefully acknowledge the funding by the Deutsche Forschungsgemeinschaft (DFG, German Research Foundation) - Projektnummer  
268020496 - TRR 172, within the Transregional Collaborative Research Center "Arctic Amplification: Climate Relevant Atmospheric and  
395 SurfaCe Processes, and Feedback Mechanisms (AC)<sup>3</sup>". We thank J. Chylik for comments that helped to improve the readability of our  
manuscript.

## References

- Aagaard, K., Coachman, L. K., and Carmack, E.: On the halocline of the Arctic Ocean, *Deep Sea Res. Part I Oceanogr. Res. Pap.*, 28, 529–545, [https://doi.org/10.1016/0198-0149\(81\)90115-1](https://doi.org/10.1016/0198-0149(81)90115-1), 1981.
- 400 Alkire, M. B., Polyakov, I., Rember, R., Pnyushkov, A., Ivanov, V., and Ashik, I.: Combining physical and geochemical methods to investigate lower halocline water formation and modification along the Siberian continental slope, *Ocean Sci.*, 13, 983–995, <https://doi.org/10.5194/os-13-983-2017>, 2017.
- Anderson, L. G., Andersson, P. S., Björk, G., Jones, E. P., Jutterström, S., and Wåhlström, I.: Source and formation of the upper halocline of the Arctic Ocean, *J. Geophys. Res. Oceans*, 118, 410–421, <https://doi.org/10.1029/2012jc008291>, 2013.
- 405 Athanase, M.: Review on the manuscript EGUSPHERE-2023-106, *EGUsphere*, <https://doi.org/10.5194/egusphere-2023-106-RC2>, 2023.
- Behrendt, A., Sumata, H., Rabe, B., and Schauer, U.: UDASH – Unified Database for Arctic and Subarctic Hydrography, *Earth Syst. Sci. Data*, 10, 1119–1138, <https://doi.org/10.5194/essd-10-1119-2018>, 2018.
- Bertosio, C., Provost, C., Sennéchaël, N., Artana, C., Athanase, M., Boles, E., Lellouche, J.-M., and Garric, G.: The western Eurasian Basin halocline in 2017: Insights from autonomous NO measurements and the Mercator Physical System, *J. Geophys. Res. Oceans*, 125, e2020JC016204, <https://doi.org/10.1029/2020JC016204>, 2020.
- 410 Bertosio, C., Provost, C., Athanase, M., Sennéchaël, N., Garric, G., Lellouche, J.-M., Kim, J.-H., Cho, K.-H., and Park, T.: Changes in Arctic halocline waters along the East Siberian Slope and in the Makarov Basin from 2007 to 2020, *J. Geophys. Res. Oceans*, 127, <https://doi.org/10.1029/2021jc018082>, 2022.
- Björk, G., Söderkvist, J., Winsor, P., Nikolopoulos, A., and Steele, M.: Return of the cold halocline layer to the Amundsen Basin of the Arctic Ocean: Implication for the sea ice mass balance, *Geophys. Res. Lett.*, 29, 1–8, <https://doi.org/10.1029/2001GL014157>, 2002.
- 415 Bourgain, P. and Gascard, J. C.: The Arctic Ocean halocline and its interannual variability from 1997 to 2008, *Deep Sea Res. Part I Oceanogr. Res. Pap.*, 58, 745–756, <https://doi.org/10.1016/j.dsr.2011.05.001>, 2011.
- Deng, G. and Cahill, L.: An adaptive Gaussian filter for noise reduction and edge detection, in: 1993 IEEE Conference Record Nuclear Science Symposium and Medical Imaging Conference, vol. 3, pp. 1615–1619, IEEE, San Francisco, CA, USA, <https://doi.org/10.1109/nssmic.1993.373563>, 1993.
- 420 Dmitrenko, I. A., Kirillov, S. A., Rudels, B., Babb, D. G., Pedersen, L. T., Rysgaard, S., Kristoffersen, Y., and Barber, D. G.: Arctic Ocean outflow and glacier–ocean interactions modify water over the Wandel Sea shelf (northeastern Greenland), *Ocean Sci.*, 13, 1045–1060, <https://doi.org/10.5194/os-13-1045-2017>, 2017.
- GEBCO Bathymetric Compilation Group 2021: The GEBCO\_2021 grid - a continuous terrain model of the global oceans and land., <https://doi.org/10.5285/c6612cbe-50b3-0cff-e053-6c86abc09f8f>, 2021.
- 425 Gill, A. E.: *Atmosphere-ocean dynamics* (International Geophysics Series, Volume 30), Academic Press, 1982.
- Jones, E. P. and Anderson, L. G.: On the origin of the chemical properties of the Arctic Ocean halocline, *J. Geophys. Res.*, 91, 10 759, <https://doi.org/10.1029/jc091ic09p10759>, 1986.
- Krishfield, R., Toole, J., Proshutinsky, A., and Timmermans, M.-L.: Automated ice-tethered profilers for seawater observations under pack ice in all seasons, *J. Atmos. Ocean Technol.*, 25, 2091–2105, <https://doi.org/10.1175/2008JTECHO587.1>, 2008.
- 430 Lind, S., Ingvaldsen, R. B., and Furevik, T.: Arctic layer salinity controls heat loss from deep Atlantic layer in seasonally ice-covered areas of the Barents Sea, *Geophys. Res. Lett.*, 43, 5233–5242, <https://doi.org/10.1002/2016GL068421>, 2016.

- Macdonald, R. W., Kuzyk, Z. A., and Johannessen, S. C.: It is not just about the ice: a geochemical perspective on the changing Arctic Ocean, *J. Environ. Stud. Sci.*, 5, 288–301, <https://doi.org/10.1007/s13412-015-0302-4>, 2015.
- 435 Metzner, E. P., Salzmann, M., and Gerdes, R.: Arctic Ocean surface energy flux and the cold halocline in future climate projections, *J. Geophys. Res. Oceans*, 125, e2019JC015554, <https://doi.org/10.1029/2019JC015554>, 2020.
- Peralta-Ferriz, C. and Woodgate, R. A.: Seasonal and interannual variability of pan-Arctic surface mixed layer properties from 1979 to 2012 from hydrographic data, and the dominance of stratification for multiyear mixed layer depth shoaling, *Prog. Oceanogr.*, 134, 19–53, <https://doi.org/10.1016/j.pocean.2014.12.005>, 2015.
- 440 Polyakov, I.: Review of the manuscript (egusphere-2023-106) entitled “Technical note: Determining Arctic Ocean cold halocline and cold halostad layer depths based on vertical stability” by E. P. Metzner and M. Salzmann, *EGUsphere*, <https://doi.org/10.5194/egusphere-2023-106-RC1>, 2023.
- Polyakov, I. V., Pnyushkov, A. V., Alkire, M. B., Ashik, I. M., Baumann, T. M., Carmack, E. C., Goszczko, I., Guthrie, J., Ivanov, V. V., Kanzow, T., Krishfield, R., Kwok, R., Sundfjord, A., Morison, J., Rember, R., and Yulin, A.: Greater role for Atlantic inflows on sea-ice loss in the Eurasian Basin of the Arctic Ocean, *Science*, 356, <https://doi.org/10.1126/science.aai8204>, 2017.
- 445 Polyakov, I. V., Pnyushkov, A. V., and Carmack, E. C.: Stability of the Arctic halocline: a new indicator of Arctic climate change, *Environ. Res. Lett.*, 13, <https://doi.org/10.1088/1748-9326/aaec1e>, 2018.
- Polyakov, I. V., Rippeth, T. P., Fer, I., Alkire, M. B., Baumann, T. M., Carmack, E. C., Ingvaldsen, R., Ivanov, V. V., Janout, M., Lind, S., Padman, L., Pnyushkov, A. V., and Rember, R.: Weakening of cold halocline layer exposes sea ice to oceanic heat in the eastern Arctic Ocean, *J. Clim.*, 33, 8107–8123, <https://doi.org/10.1175/JCLI-D-19-0976.1>, 2020.
- 450 Roquet, F., Ferreira, D., Caneill, R., Schlesinger, D., and Madec, G.: Unique thermal expansion properties of water key to the formation of sea ice on Earth, *Sci. Adv.*, 8, <https://doi.org/10.1126/sciadv.abq0793>, 2022.
- Rudels, B., Anderson, L. G., and Jones, E. P.: Formation and evolution of the surface mixed layer and halocline of the Arctic Ocean, *J. Geophys. Res. Oceans*, 101, 8807–8821, <https://doi.org/10.1029/96JC00143>, 1996.
- 455 Rudels, B., Jones, E. P., Schauer, U., and Eriksson, P.: Atlantic sources of the Arctic Ocean surface and halocline waters, *Polar Res.*, 23, 181–208, <https://doi.org/10.3402/polar.v23i2.6278>, 2004.
- Shimada, K., Itoh, M., Nishino, S., McLoaghlin, F., Carmack, E., and Proshutinsky, A.: Halocline structure in the Canada Basin of the Arctic Ocean, *Geophys. Res. Lett.*, 32, <https://doi.org/10.1029/2004GL021358>, 2005.
- 460 Steele, M. and Boyd, T.: Retreat of the cold halocline layer in the Arctic Ocean, *J. Geophys. Res.*, 103, 10419–10435, <https://doi.org/10.1029/98JC00580>, 1998.
- Steele, M., Morison, J., and Curtin, T.: Halocline water formation in the Barents Sea, *J. Geophys. Res.*, 100, 881–894, 1995.
- Timmermans, M.-L., Proshutinsky, A., Golubeva, E., Jackson, J. M., Krishfield, R., McCall, M., Platov, G., Toole, J., Williams, W., Kikuchi, T., and Nishino, S.: Mechanisms of Pacific Summer Water variability in the Arctic's Central Canada Basin, *J. Geophys. Res. Oceans*, 119, 7523–7548, <https://doi.org/10.1002/2014jc010273>, 2014.
- 465 Toole, J. M., Krishfield, R. A., Timmermans, M.-L., and Proshutinsky, A.: The ice-tethered profiler: ARGO of the Arctic, *Oceanography*, 24, 126–135, <http://www.jstor.org/stable/24861307>, 2011.
- Zhong, W., Steele, M., Zhang, J., and Cole, S. T.: Circulation of Pacific Winter Water in the Western Arctic Ocean, *J. of Geophys. Res. Oceans*, 124, 863–881, <https://doi.org/10.1029/2018jc014604>, 2019.